

Extending range through Structured Back Focal Plane Interferometry

Avinash Upadhyaya^{*a}, Yujie Zheng^a, Li Li^b, Woei Ming Lee^a

^aJohn Curtin School of Medical Research, 121 Garran Road, Canberra, ACT, Australia 2601;

^bThe State Key Laboratory of Optoelectronic Materials and Technologies, Sun Yat-sen University, Guangzhou, China 510275

ABSTRACT

Back Focal Plane interferometry (BFPI) is a widely used technique in particle tracking, providing high-speed, high-resolution measurements. We present Structured Back Focal Plane Interferometry (SBFPI), a modification to BFPI utilizing structured beams and structured detectors [1]. Utilising Conical Wavefront Gaussian Beams and Annular Quadrant Photodetectors, SBFPI significantly increases tracking range while maintaining sensitivity and robustness to aberrations. We studied the variation in detection range and sensitivity over our parameters. A maximum increase in axial and lateral tracking range of 4.25-fold and 1.83-fold was found respectively, concomitant with sensitivity decreases of 53% and 61%. We also found parameter combinations with smaller range improvements but which retain sensitivity, in particular a 2.31 fold axial range increase with a 22.4% reduction in sensitivity, and these can be tuned to each experiment. We also studied the effect of aberrations on signal integrity.

Keywords: Back Focal Plane Interferometry, Conical Wavefront, Gaussian Beam, Structured Light

1. INTRODUCTION

1.1 Overview of Back Focal Plane Interferometry

Back Focal Plane Interferometry (BFPI) is a well-established technique for 3D particle tracking, with the ability to make nanometer scale and MHz rate measurements [2]. There have been numerous prominent examples of BFPI being used for high precision measurements of force and position [3-5]. As an example, in [5] they studied the movement of a single kinesin molecule along a microtubule track, visualizing the 8 nm step movement of the molecule and determining that each step was associated with the hydrolysis of an ATP molecule. Such studies demonstrate the powerful sensitivity of BFPI for measurements at the nanoscale.

A typical BFPI setup is presented in Figure 1A. The setup consists of an optical train in which a gaussian laser source is brought to a focus. The particle of interest can move within this focal volume, scattering a portion of this light. In parallel, a proportion of the light moves through the system unaffected by the particle. The BFPI pattern arises from the interference of these scattered and non-scattered components of the beam at the back focal plane of the detection lens [2]. A lens then relays this back focal plane intensity to the detector. This BFPI pattern contains information of the full three-dimensional position of the particle, which can be extracted using a Quadrant Photodetector (QPD) [6]. An example of a BFPI intensity pattern that is present at the plane of the detector is given in Figure 1B, where the QPD splits up the pattern into four quadrants. The BFPI signals for particle position along each axis can be determined using the equations in Figure 1C, which are then plotted against the particle position to obtain a calibration curve. An idealized example of an axial calibration curve is presented in Figure 1D. The curve has a quasi-linear region which can be used for particle tracking, and from which we can extract two key parameters: *range* and *sensitivity*. These characterize a BFPI measurement setup, where the range is the distance over which the particle can move while remaining in the linear region, and the sensitivity is the gradient of this region which determines detection resolution.

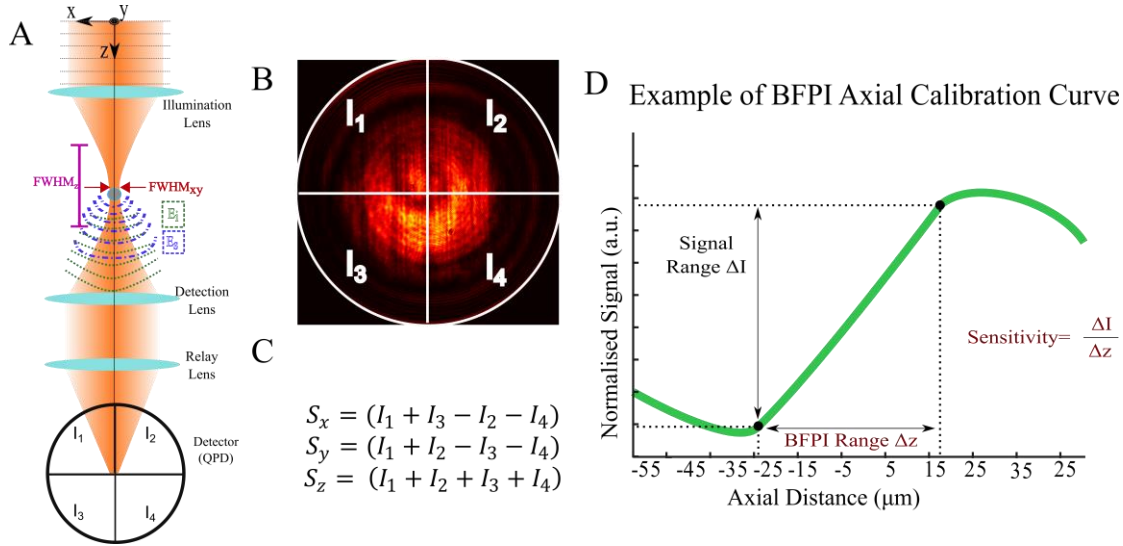


Figure 1 - The construction of a typical BFPI setup. A) The optical train involving a gaussian beam, illumination lens, particle of interest, detection lens, relay lens, and quadrant photodetector (QPD) where E_i and E_s are the non-scattered and scattered light respectively, **B)** An example of the BFPI Pattern and its segmentation via the QPD. **C)** The QPD quadrants can be processed via these equations for the lateral (S_x , S_y) and axial (S_z) BFPI signals. **D)** An example of an axial calibration curve, where the S_z signal is plotted against the axial position of the particle. Portions of this figure are adapted from [1].

As an on-axis interference effect, the BFPI intensity pattern is highly complex. Its interferometric nature means detection rate is limited only by the detector allowing us to achieve MHz rates using photodetectors and also is sensitive to minute changes in particle position [2]. As an interference pattern, however, the precise form of the BFPI intensity pattern is affected by parameters ranging from the beam profile at the focus, the properties of the particle being tracked such as the refractive index and particle size, the optics in the train, among others. This situation makes it very difficult to predict, meaning that it is highly difficult to tune the behaviour of the system, i.e. to vary the range and sensitivity as required.

1.2 Increasing tracking range, while maintaining sensitivity

Increases in range are highly desirable for BFPI. For example, force is proportional to displacement for a bead trapped in an optical potential. The ability to track a particle over a larger range means that larger forces can be measured. Tunability would also be a useful factor, as a single setup can be tailored to the sample at hand. There have been numerous examples of extending range in the literature, such as by introducing a second tracking focus in the same setup [7], increasing the focal volume by reducing illumination lens numerical aperture [8], as well as introducing a stop at the plane of the BFPI signal [9]. These usually increase the complexity of the setup, and many of the range improvements achieved by such methods can come with an additional drawback: a loss in sensitivity.

The reason for this is that the range and the sensitivity are affected by the intensity profile of the illumination beam (lateral and axial beam intensities), as well as the Gouy phase. These relationships are described in [2] as below:

$$\frac{I_{\text{BFPI}xy}}{I_{\text{total}}}(x) \propto \left(\frac{x}{FWHM_{x,y}^2}\right) e^{(-x/FWHM_{x,y})^2} \quad (1)$$

$$\frac{I_{\text{BFPI}z}}{I_{\text{total}}}(z) \propto \left(\frac{1}{FWHM_{x,y}^2}\right) \left(1 + \left(\frac{z}{FWHM_z}\right)^2\right)^{-1/2} \sin(\alpha), \quad \text{where } \alpha = \tan^{-1}(z/FWHM_z) \quad (2)$$

Equations (1) and (2) describe the lateral and axial BFPI sensitivities. Sensitivities in both lateral and axial directions are affected by the beam waist at the focus denoted as the $FWHM_{xy}$. This explains why reducing illumination NA reduces sensitivity – if one were to double the beam waist, this would result in an 8-fold decrease in sensitivity laterally and 4-fold axially. Also for the axial case, there is an additional factor α which denotes the axial progression of the Gaussian beam as it focuses. This can be seen to be the Gouy phase, an effect in which a gaussian beam in a 2D focus (as in our case) develops an integrated phase difference of π compared to an equivalent plane wave [10]. The Gouy phase is a well-

known phenomenon and has been studied extensively, with numerous analyses of its origin [10-12]. It results from the transverse spatial confinement of the beam at the focus which leads to a distribution in transverse momenta. This distribution changes the expectation value for the axial propagation constant [10] and produces the characteristic phase difference. From equation (2) we can see that the Gouy phase is essential to axial BFPI sensitivity. The Gouy phase requirement also rules out the use of Bessel beams, as they have minimal Gouy phase [13]. Their generation from annularly converging oblique plane waves means there is no focusing and hence minimal phase progression along the optical axis [13]. Therefore, while the extended axial intensity should intuitively increase BFPI range, equation (2) implies that there would be minimal sensitivity due to the lack of Gouy phase.

Hence in summary, for BFPI with extended range and minimal loss in sensitivity, it is necessary to (1) extend the axial intensity of the illumination beam, (2) maintain or reduce the beam waist at the focus, and (3) Gouy phase must be preserved.

1.3 Our approach: Structured Back Focal Plane Interferometry

We incorporated structured beams and structured detectors into a BFPI setup, a combination we call Structured Back Focal Plane Interferometry (SBFPI) [1]. On the illumination side, we modulated a gaussian beam with a conical phase before the illumination lens, which we call the Conical Wavefront Gaussian Beam (CWGB). The CWGB had the effect of elongating the focus in the axial direction while still maintaining the Gouy phase progression. On the detection side, we incorporated the proposal in [9] by blocking the central portion of the BFPI pattern, a detection scheme referred to as an Annular QPD (AQPD). We integrated these aspects into a BFPI setup and in a series of experiments, we analysed the suitability of the CWGB and AQPD for BFPI. We found that the SBFPI configuration increases tracking range and also improves resilience to spatial aberrations in the optical train.

2. SIMULATION

We first conducted numerical simulations to analyse the phase and intensity profiles of the CWGB, and compare them to a gaussian and quasi-bessel. We first define the different phase and amplitude modulation schemes that produce our beam profiles. We place these profiles at the back focal plane of our illumination lens. As can be seen in Figure 2A i, the CWGB is produced via application of a linear radial phase across the width of the beam with a standard gaussian amplitude. This is different from a typical gaussian focus which is produced using a gaussian amplitude but a flat phase as in Figure 2A ii. Unlike both the CWGB and gaussian, the Quasi-Bessel beam (QBB) is produced with an amplitude mask in the form of an annular ring.

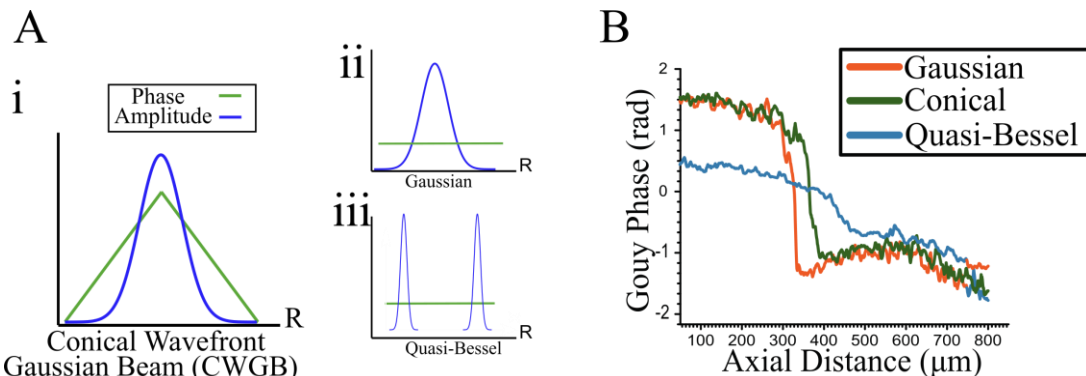


Figure 2 – A) Beam profiles for the Conical Wavefront Gaussian Beam (CWGB), Gaussian, and Quasi-Bessel Beam (QBB). B) Plot of phase progression along the optical axis against axial position of the particle. Portions of this figure adapted from [1].

We used a numerical Fourier split-step simulation using the beam profiles described previously and a thin lens with phase factor $\exp(-i \frac{k}{2f} r^2)$, where f is the focal length, r is the radial position perpendicular to the optical axis. This thin lens model does not consider non-paraxial rays but it does provide a qualitative comparison of the $FWHM_{xy}$, $FWHM_z$, and Gouy phase α . We used the gaussian as a standard of comparison for BFPI. Firstly for the QBB, we used an annular ring thickness of 11% of the pupil of the lens, which exhibited an elongated axial focus with an increase in a 3.5-fold increase in $FWHM_z$ compared to the gaussian. The QBB also had minimal change in its beam waist (<10%). The overall signal, however, decreased by a factor of 4. Most importantly, as can be seen in Figure 2B the gouy phase progression is

markedly different from the case of the gaussian. For the gaussian, we see a sharp jump across the focus, whereas the progression for the QBB is much slower.

The conical phase for the CWGB was parametrized as $\phi = 2\pi r/d_c$ where r is the radial parameter and d_c determines the slope of the radial linear phase. Our intuition for this case was that the marginal and paraxial rays would be brought to a focus at different points along the optical axis, hence producing an elongated focal depth. In our simulations we used a $d_c=0.12$. As expected, the simulation showed an elongation of $FWHM_z$ by factor 2.2, a significant but more modest improvement compared to the QBB. We also found that the beam waist was also maintained within 10%. Looking at Figure 2B, however, we see that the gouy phase jump present in the gaussian is still present in the CWGB. This indicates that the CWGB is suitable for use in BFPI as given by our previously stated requirements. Further details of our simulation can be found in [1].

3. EXPERIMENTAL SETUP

We constructed a test setup to explore the parameters of SBFPI as shown in Figure 3A. We expanded our beam to overfill the active area of our Spatial Light modulator (Meadowlark optics, 7.68x7.68mm, incident angle 18°) conjugated via 4f system to the back focal plane of the illumination lens (N.A. 0.3, 10x). An iris (not shown) was used to select the first order of a blazed grating applied to each phase mask. This allowed us to introduce spatial aberrations, vary the conical wavefront phase angle, and permits 3D beam steering at high precision. A higher NA detection lens (N.A. 0.8, 40x) was used to generate the BFPI signal at its back focal plane, which was relayed by a 30 mm focal length lens to the plane of a digital camera (Pixelfly USB, PCO). To produce the BFPI signal, we used a bead (polymer, diameter 3 μm, n=1.59, Polysciences Inc) air-dried onto glass slides and moved into the focus of the beam.

For the axial BFPI case, we could generate calibration curves by moving the bead using an XYZ stage (Thor Labs XYFM1, DDSM100/M), for the lateral directions we used the remote steering capability of the SLM to move the focus relative to the bead. Our lateral resolution in moving our focus was in ~363 nm step sizes, whereas in the axial direction our resolution was given by the stage resolution of ~1 μm. For the detection, our CCD camera allows us to visualize the BFPI pattern and apply pixel binning to vary the detection scheme. Unlike traditional detectors, the pixel binning schemes allows us to compare the effect of the traditional QPD with the AQPD detection scheme discussed previously.

An example of a conical wavefront phase mask is shown in Figure 3B i and corresponding line profiles in Figure 3B ii. As described previously, the conical phase is given by $\phi = 2\pi r/d_c$ and so lower d_c values correspond to higher radial phase gradient. For the detection, an example of the annular detection scheme is seen in the context of a BFPI pattern. The size of the central region divided by the total diameter is given by the A parameter. $A=0$ corresponds to traditional QPD detection where no intensity is blocked, whereas for example, $A=0.5$ means 0.5% of the radius is blocked. All of the following experiments relied on the same bead size, and calculation from the quadrants as given in Figure 1C.

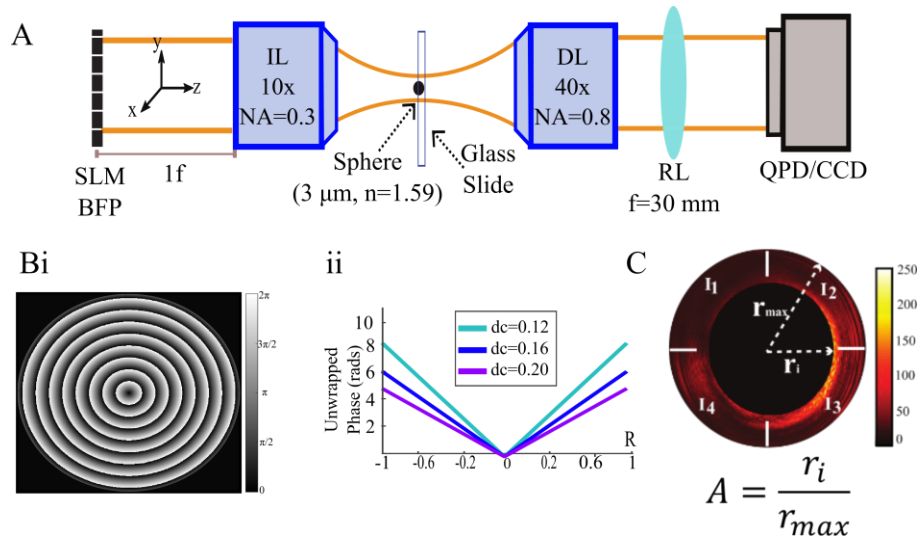


Figure 3 – A) Structured Back Focal Plane Interferometry (SBFPI) optical setup, B) i) illustration of the conical phase mask, ii) line profile of the phase mask, C) Illustration of the AQPD detection and parameter. Figure adapted from [1]

4. RESULTS

4.1 Effect of the CWGBs on Extended Axial Detection in BFPI

As described in the previous section, we imparted a range of conical wavefronts to our beam as well as a flat phase for the gaussian case. Moving our bead axially through the focus in each case, we generated a set of calibration curves corresponding to different beam profiles, the normalized versions of which are given in Figure 4A.

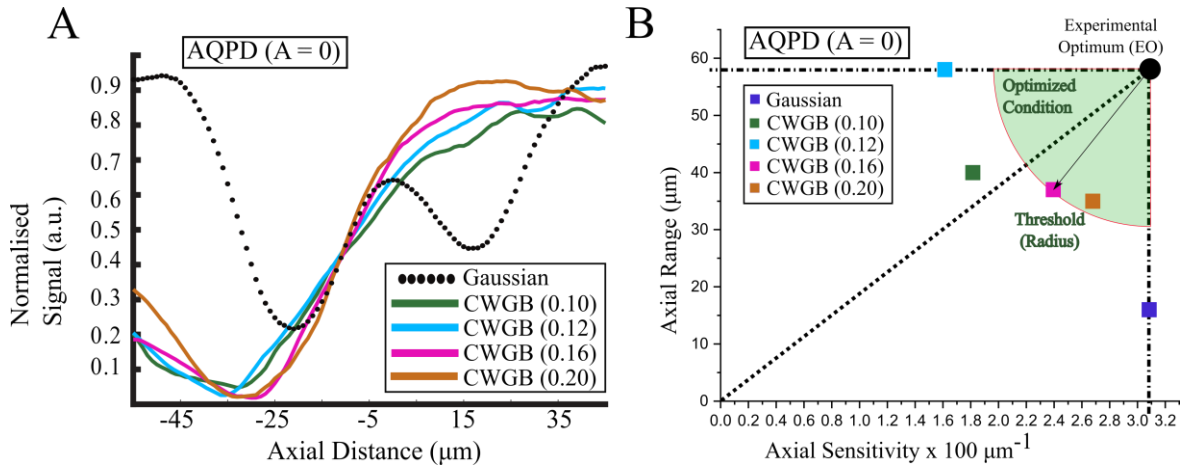


Figure 4 - Results of experiments studying the effect of CWGBs on axial BFPI detection. Traditional QPD detection given by $A=0$ was used in all cases. Figure adapted from [1].

As can be seen in Figure 4A, the results for all the CWGBs extended the linear range of the method compared to the gaussian case. To quantify the improvement in range and sensitivity for each case, we used the linear least squares method in the Matlab Curve Fitting Toolbox with a goodness of fit threshold of $R^2=0.97$. From this, we could extract the gradient (sensitivity) and the linear range from the region used with the fitting model. We plotted the range and sensitivity of the beam profile in a scatter plot in Figure 4B. From this scatter plot, we can see that compared to the gaussian case given by blue, we achieved a range increase from 16 to 58 μm (~ 3.63 -fold improvement) for the $d_c=0.12 \text{ rad}^{-1}$ case. Unfortunately, this was accompanied by a $\sim 48\%$ decrease of sensitivity, which may arise from changes to the beam waist.

Using the best range point ($d_c = 0.12 \text{ rad}^{-1}$) and the best sensitivity point (gaussian), we constructed a hypothetical data point called the Experimental Optimum (EO). We used distance from this point as a figure of merit for each data point, with points above the diagonal favouring range increase and points below favouring sensitivity increase. Through this found the $d_c=0.16 \mu\text{m}^{-1}$ had the best balanced improvement, a 2.31 fold range extension with a 22.4% decrease in sensitivity. Nevertheless, we note that while all CWGB points experienced range improvements, they also had sensitivity losses compared to the gaussian.

4.2 Recovering Sensitivity for Axial detection in BFPI

Given that all CWGB profiles experienced sensitivity loss, we investigated whether the AQPDP parameter was able to offset this loss. We conducted a similar experiment to the previous section, but we varied the AQPDP parameter while keeping the d_c parameter fixed at 0.16 rad^{-1} . The calibration curves and associated sensitivity plot are given in Figure 5, with display and data processing conducted in the same way as the previous section. We also retained the Gaussian dataset under traditional detection in the scatter plot for comparison.

We found the $A=0.7$ dataset to be closest to the EO and hence has the best performance with a range increase of factor 2.31 and a 1.2% increase in intensity compared to the gaussian. If we compare this with the $A=0$ (traditional QPD detection case), we see that the range increase is identical, but that experienced a 22.4% reduction in sensitivity. The $A=0.2$ case even had an increased range of 68 μm albeit with a sensitivity loss of $\sim 52\%$ compared to the gaussian.

In summary, this shows that the AQPDP detection scheme can recover detection sensitivity in axial BFPI, and in some cases produce range increases also.

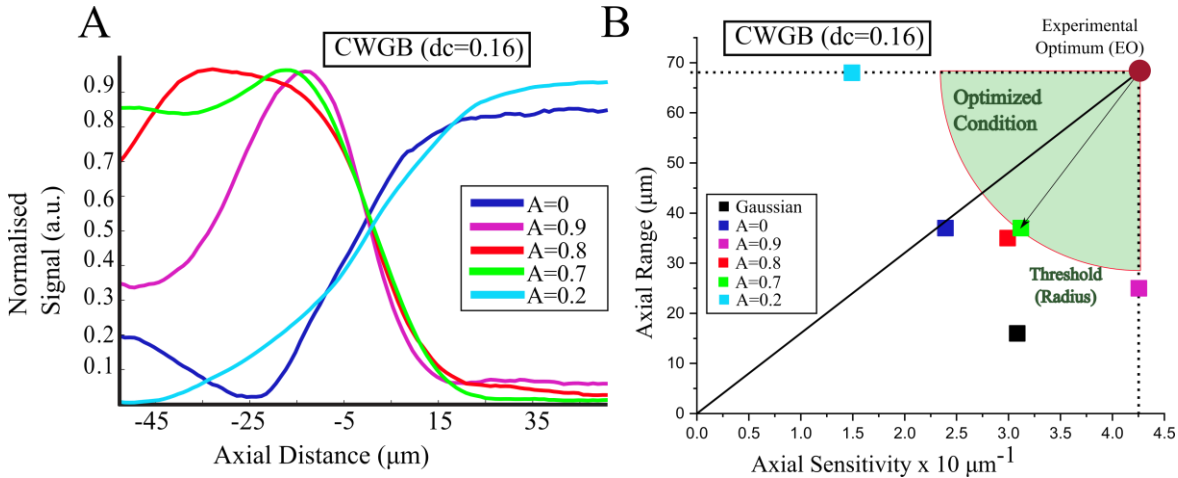


Figure 5 - Effect of AQPDP detection on axial BFPI. CWGB with $d_c=0.16 \text{ rad}^{-1}$ was used for all cases except the reference gaussian. $A=0$ CWGB corresponds to the traditional QPD detection and serves as a benchmark for the CWGB datasets. Figure adapted from [1].

4.3 Effects of CWGB and AQPDP on lateral BFPI

While previously we investigated the axial BFPI signal, in this case, we studied the effect of our CWGB on the lateral signal. The lateral signal was calculated using the differential signal calculated as in Figure 1C. In these experiments, rather than moving the bead through a static beam focus, we employed the SLM to steer the focus incrementally around a bead. This had an equivalent effect on the BFPI signal, and by measuring the lateral BFPI signal for each beam position, we could generate calibration curves as in the previous experiments. Processing and plotting were conducted as described earlier.

We again used a $d_c=0.16 \text{ rad}^{-1}$ parameter while changing the AQPDP parameter. The best CWGB dataset was found to be the $A=0.7$, which presented a 1.67-fold range increase with a sensitivity loss of 51%. Interestingly, the dataset closest to the EO was the gaussian. Looking more closely at the scatter plot, we can see that the CWGB with $A=0$ produces no range increase, but a large $\sim 72\%$ decrease. The additional use of A parameters on this dataset recovers some of the sensitivity but increases the range significantly as seen for example in the $A=0.9$ point.

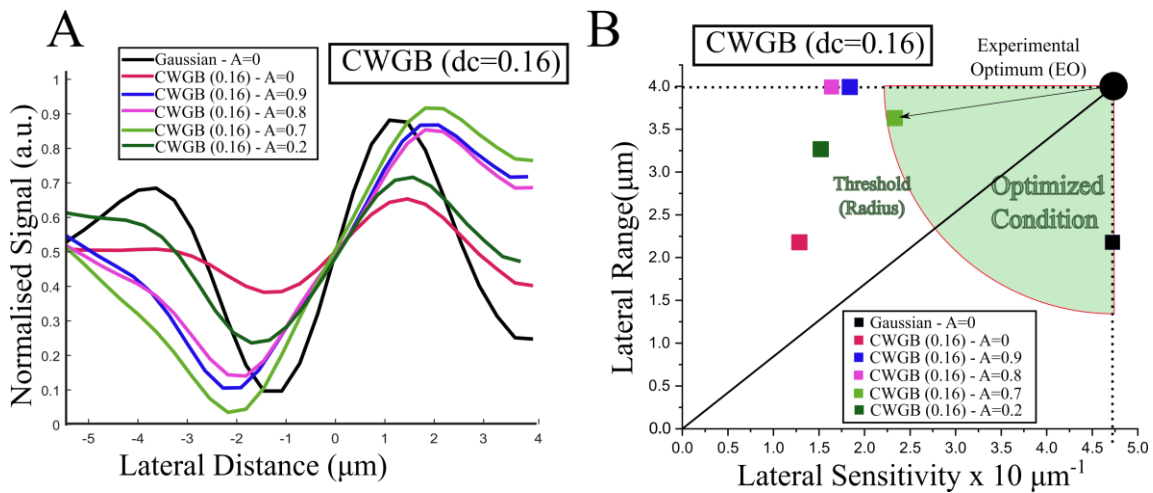


Figure 6 - Effect of the CWGB and AQPDP on lateral BFPI. We used CWGBs with 0.16 rad^{-1} for all cases except the reference gaussian. The $A=0$ CWGB corresponds to traditional QPD detection and serves as a benchmark for the CWGB datasets. Figure adapted from [1].

4.4 Resilience against Spatial Aberrations

As the BFPI signal contains the full 3D information of the tracked particle, aberrations can induce crosstalk between position measurements along each axis [14]. In the case of SBFPI, as we shape our CWGB beams, aberrations could distort our focal intensity. We first corrected for system aberrations as in [15] and in a series of experiments, we introduced controlled amplitudes of astigmatism via our SLM. In all these cases we used a CWGB of $d_c=0.16 \text{ rad}^{-1}$ as before and obtained a series of calibration curves corresponding to the application of each astigmatism amplitude. We repeated this procedure for $A=0$ and $A=0.7$ detection, and through this, we could see the effect of the AQPd detection on aberrated CWGBs. In Figure 7A i we can see that the application of aberration severely skews the curves compared to the non-aberrated case, but the use of the $A=0.7$ detection restores the behaviour of the curves for all aberrations except the $+0.80\lambda$. We believe this results from the asymmetry of the intensity distortion for different signs, meaning that both the magnitude and sign of the astigmatism amplitude need to be taken into account. Analysing the linear regions for all curves, we found that in all cases the AQPd detection recovered sensitivity compared to the QPD, illustrating the resilience of SBFPI to spatial aberrations.

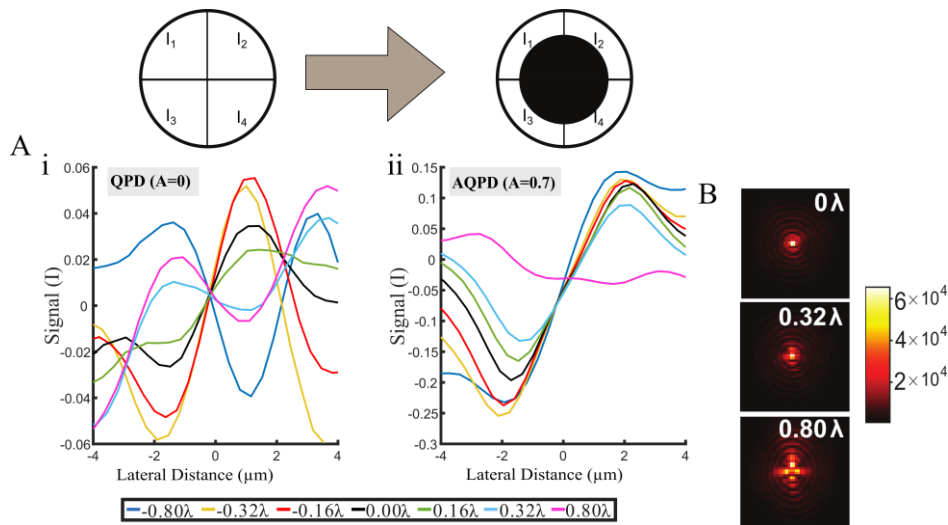


Figure 7 – Investigating the effect of aberrations (astigmatism) on CWGB coupled with AQPd detection in lateral BFPI. All datasets used $d_c=0.16 \text{ rad}^{-1}$. A i) shows calibration curves for QPD detection, ii) shows the calibration curves for $A=0.7$. B) shows examples of the effect of different astigmatism amplitudes on the intensity profiles at the focus. Figure adapted from [1].

5. REFERENCES

- [1] A. Upadhyaya, Y. Zheng, L. Li *et al.*, “Structured Back Focal Plane Interferometry (SBFPI),” *Scientific Reports*, 9(1), 20273 (2019).
- [2] A. Pralle, M. Prummer, E. L. Florin *et al.*, “Three-dimensional high-resolution particle tracking for optical tweezers by forward scattered light,” *Microscopy Research and Technique*, 44(5), 378-386 (1999).
- [3] M. W. Allersma, F. Gittes, M. J. deCastro *et al.*, “Two-Dimensional Tracking of ncd Motility by Back Focal Plane Interferometry,” *Biophysical Journal*, 74(2), 1074-1085 (1998).
- [4] J. T. Finer, A. D. Mehta, and J. A. Spudich, “Characterization of single actin-myosin interactions,” *Biophysical journal*, 68(4 Suppl), 291S-297S (1995).
- [5] K. Visscher, M. J. Schnitzer, and S. M. Block, “Single kinesin molecules studied with a molecular force clamp,” *Nature*, 400(6740), 184-189 (1999).
- [6] A. Rohrbach, and E. H. Stelzer, “Three-dimensional position detection of optically trapped dielectric particles,” *Journal of Applied Physics*, 91(8), 5474-5488 (2002).
- [7] L. Friedrich, and A. Rohrbach, “Improved interferometric tracking of trapped particles using two frequency-detuned beams,” *Optics Letters*, 35(11), 1920-1922 (2010).

- [8] I. A. Martínez, and D. Petrov, "Back-focal-plane position detection with extended linear range for photonic force microscopy," *Applied Optics*, 51(25), 5973-5977 (2012).
- [9] S. M. Mousavi, S. Akbar, H. Faegheh *et al.*, "Extended linear detection range for optical tweezers using a stop at the back focal plane of the condenser," *Journal of Optics*, 17(6), 065606 (2015).
- [10] S. Feng, and H. G. Winful, "Physical origin of the Gouy phase shift," *Optics Letters*, 26(8), 485-487 (2001).
- [11] R. W. Boyd, "Intuitive explanation of the phase anomaly of focused light beams," *Journal of the Optical Society of America*, 70(7), 877-880 (1980).
- [12] P. Hariharan, and P. A. Robinson, "The gouy phase shift as a geometrical quantum effect," *Journal of Modern Optics*, 43(2), 219-221 (1996).
- [13] M.-S. Kim, T. Scharf, A. d. C. Assafrao *et al.*, "Phase anomalies in Bessel-Gauss beams," *Optics Express*, 20(27), 28929-28940 (2012).
- [14] T. F. Dixon, L. W. Russell, A. Andres-Arroyo *et al.*, "Using back focal plane interferometry to probe the influence of Zernike aberrations in optical tweezers," *Optics Letters*, 42(15), 2968-2971 (2017).
- [15] N. Eckerskorn, W. Krolikowski, L. Li *et al.*, [Optical control over particle transport in air and in vacuum: Quantifying forces by particle levitation] Australian National University, Canberra(2014).